Modular Passivity-Based Modeling of Piezoelectric Actuators

Ignacio Díaz^{a,b}, Héctor Ramírez^a, Yann Le Gorrec^b, Yongxin Wu^b

^aDepartamento de Electrnica Universidad Tcnica Federico Santa Maria Valparaso Chile b Universite Marie et Louis Pasteur SUPMICROTECH CNRS institute FEMTO-ST F-25000 Besancon France

Abstract

This paper is concerned with the constructive, modular and easy to implement passivity-based rate-dependent modelling of piezoelectric actuators (PZAs) using the port Hamiltonian (PH) framework. The proposed model incorporates hysterons to capture the hysteresic behavior of PZAs, resulting in a causal bond-graph representation and a simplified explicit PH formulation. The proposed model is an input-affine port-Hamiltonian system that is shown to be asymptotically stable with respect to an arbitrary equilibrium configuration. The model is experimentally validated over a large range of operation frequencies using a commercial piezoelectric actuator and compared to a Bouc-Wen model of the same order.

Keywords: Port-Hamiltonian system, Hysteresis, Piezoelectric Actuator, Nonlinear Control System, Passivity

1. Introduction

In this work, we propose a passivity-based, rate-dependent (in the sense that the hysteresis shape depends on the shape of the input between two extrema) model for piezoelectric actuators (PZAs) using the port Hamiltonian (PH) framework. The model incorporates hysterons to capture the hysteresic behavior of PZAs, resulting in a causal bond-graph representation and a simplified, explicit PH formulation.

Piezoelectric materials are characterized by their coupled electric and mechanical response. In recent years, due to the high resolution motion capabilities of PZAs various applications have been explored. These include applications in fuel injectors [1], hydraulic valves [2], atomic force microscopes [3], different medical applications and bionic actuators [4, 5]. Additionally, PZAs have found applications in computer components [6], adaptive optics [7] and micro manipulators [8, 9]. In many of these applications, various models are used to describe the nonlinear behavior of the PZ materials. One of the main challenges is addressing the hysteresis between the input voltage and the mechanical displacement of the actuator. This phenomenon has been modeled using a variety of methods, as presented in [10]. Most of the proposed solutions involve piecewise functions such as the basic hysteresis operator from the Preisach model [10], the min and max operators in the Prandtl-Ishlinskii method [11] and in the Duhem model [12], the absolute value function in the Bouc-Wen approach [13, 14, 15, 16], and the sign function in the Maxwell Resistive Capacitor [17, 18]. Aforementioned hysteresis modeling methods can be categorized into two main types: rateindependent models, such as the Preisach model, the Prandtl-Ishlinskii model, and the Maxwell Resistive Capacitor model,

Email addresses: ignacio.diazal98@gmail.com (Ignacio Díaz), hector.ramireze@usm.cl (Héctor Ramírez), yann.le.gorrec@ens2m.fr (Yann Le Gorrec),

yongxin.wu@femto-st.fr(YongxinWu)

and rate-dependent models, such as the Bouc-Wen and Duhem models. This classification reflects whether the hysteresis response of a system depends solely on previous extreme values (rate-independent), or if the input path, including its rate, affects the shape of the hysteresis loop (rate-dependent). The use of PZA requires precise position control, which has been the focus of numerous techniques. Feedback-based control strategies have been reported with satisfactory results [19], and some have included additional anti-windup and saturation components [8]. The drawback of feedback strategies lie in their need for precise sensors, which can be costly and bulky due to the necessary accuracy and bandwidth. Consequently, alternative strategies based on feedforward control in combination with feedback, or direct feedforward control, have been investigated [20, 13, 14]. In these cases, the selection of the model used to predict the hysteresis from the aforementioned options greatly influences control performance, and the identification data are equally crucial due to the frequency and temperature-dependent response of the PZA [21, 22, 23, 24, 25, 11, 26]. In recent years, data-based modeling has garnered attention for capturing the hysteresis behavior of PZAs and other structural and mechanical systems. A comprehensive review of these methods, along with a comparison to traditional model-based approaches, is provided in [27].

The port-Hamiltonian System (PHS) framework is a mathematical formulation that allows for modeling multi-physical systems, characterized by a precise mathematical structure [28, 29]. Several PH formulations have been used to model smart material transducers with strong nonlinearities and hysteresis, such as magnetic shape memory alloys and piezoelectric materials and actuators [30, 31, 32, 33, 25]. This approach considers the energy conservation principle allowing for inherent passive systems. This property can be leveraged in the design of passivity based controllers, such as the energy shaping by control by interconnection [34]. However, this property in hysteresis modeling has only been addressed in a few works on rate-dependent hysteresis modeling, such as the Duhem hysteresis operator [35] and the Bouc-Wen hysteresis operator [36], and these works impose some strong conditions. The first attempt at PH modeling of PZA was investigated in [37] using the Maxwell hysteresis model. However, in that work, only the mechanical part of the PZA is in the PH formalism, while the hysteresis modeling remains outside the PH structure due to the causality issue raised by the Maxwell Resistive Capacitor [17]. As a consequence, the passivity of the overall model is not established.

In this paper, we aim to propose a rate-dependent PH model for a class of PZAs, which allows for the description of the hysteresis phenomenon within these actuators. Additionally, we can easily demonstrate the passivity of the proposed model. This model consists of a mechanical subsystem, formed as a mass-spring damper, interconnected with an electrical subsystem, that takes into account the hysteresis of the PZA. To present the hysteresis phenomenon, an elemental hysteresis operator called "hysteron" is used which is composed by a nonlinear admittance and an energy accumulating component [38]. This approach has been used to develop classes of thermo-mechanical models for PZA in [25]. In this paper we develop in a systematic manner a mechanical PH model which takes into account the hysteresis of the actuator which is comparable to classical hysteresis models, such as the Bouc-Wen model. One of the main benefits of the proposed PH model is that it is passive and asymptotically stable with respect to a non-zero equilibrium configuration. The PH model is derived using Bond-Graphs, hence it is direct to evaluate other possible model configurations, which are also discussed. The proposed formulation is used to model a commercial PZA, namely PB4VB2S from Thorlabs [39], and it is experimentally validated and compared with a Bouc-Wen model of the same actuator over a wide range of frequencies.

The paper is organized as follows: Section 2 derives a model of a class of PZA using Bond-Graph and PHS. Section 3 experimentally validates the proposed model and compares it with a Bouc-Wen model. Finally, Section 4 summarizes the results and outlines future work.

2. Port-Hamiltonian System Formulation

The class of PZA under study is the piezoelectric benders (PZB). These actuators consist of one or more layers of piezoelectric material connected to electrodes. When a voltage is applied, it creates an electric field within the piezoelectric material inducing a mechanical deformation as shown in Figure 1. Like other PZA, the PZB exhibits hysteresis between the input voltage V_{in} and the mechanical deformation q [10]. Furthermore the PZB does not present an unique equilibrium point for an input voltage, but rather a set of equilibrium points, hence control is usually needed [40]. Due to its passive properties, The PHS is beneficial for the stability analysis and control design. Therefore, the PH formulation of PZA appears promising when considering nonlinear control design, especially passivity-based control [34].

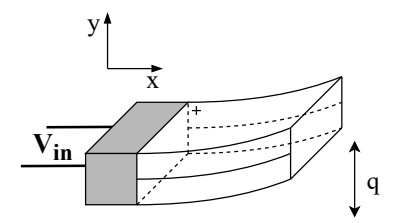


Figure 1: Piezoelectric Bender Diagram.

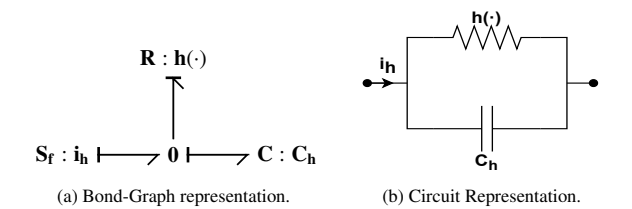


Figure 2: RC parallel hysteron.

2.1. Hysteresis Modeling

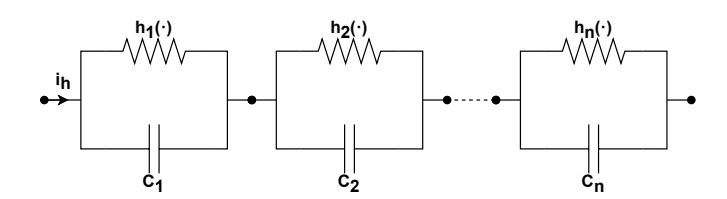


Figure 3: HRC hysteresis block.

In this paper an approach based on hysterons [38] is used for modeling the hysteresis behavior of the actuator. The approach consists in using a nonlinear resistive element paired with an energy storage element to emulate the hysteresis of the system. The advantage of the hysteron is that it corresponds to a passive subsystem. Therefore, when the hysteron is interconnected with a passive system, the overall system remains passive [38]. For the PZB under consideration, hysteresis is included in the electrical domain to simplify the mechanical domain for a posterior identification process. For the proposed model, a nonlinear resistance is connected to a linear capacitor in a parallel circuit configuration as presented in Figure 2. As discussed in [38, 25], it is possible to incorporate multiple hysterons to generate more complex hysteresis curves. The hysteresis block obtained by interconnecting n parallel RC hysterons will be denoted as Hysteron RC (HRC) block as shown in Figure 3.

When the charges Q_i in the capacitors are taken as the state variables of the HRC block system, and using the constitutive equations for the components, the dynamic equations that rule the HRC block are the following

$$\dot{Q}_i = i_h - h_i^{-1}(Q_i/C_i),$$
 (1)

for every hysteron i, where the nonlinear damping function $h_i^{-1}(\cdot)$ maps $\mathbb{R}^+ \to \mathbb{R}_0^+$ and $\mathbb{R}^- \to \mathbb{R}_0^-$ to avoid a negative entropy generation and hence a violation of the second law of Thermodynamics. This definition permits the existence of multiple zeros

in the damping function, which in turn allows the modeling of the equilibrium point set. Additionally, it is important to underline that all the points where the damping function h_i^{-1} is identically zero are in a neighborhood of (0,0), implying that the equilibrium points of the system belong to a connected set.

An example of h_i^{-1} is constructed considering the nonlinear resistive function

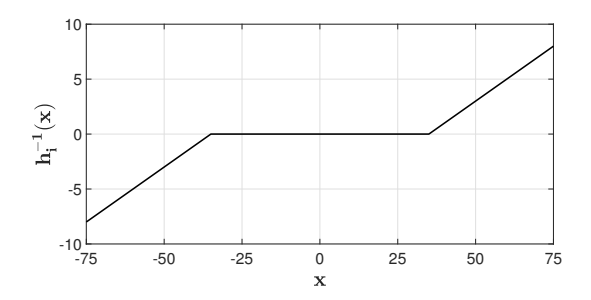


Figure 4: Example of a nonlinear damping function.

$$h_i^{-1}(x) = \begin{cases} \varrho_i^{-1} \cdot (x + d_i/2), & x < \frac{-d_i}{2} \\ 0, & \frac{-d_i}{2} \le x \le \frac{d_i}{2} \end{cases}$$
 (2)
$$\varrho_i^{-1} \cdot (x - d_i/2), & x > \frac{d_i}{2}$$

whose response with arbitrary values is shown in Figure 4.

2.2. Actuator Model

The complete PZA model comprises of a possible linear mass-spring-damper model interconnected with a nonlinear electric dynamic system through an ideal transductor element as shown in Figure 5. The nonlinear electrical system is composed of a capacitor, the HRC block and the transductor element in a series circuit connection. The proposed model is similar to the Maxwell Resistive Capacitor (MRC) model presented in [17], but instead of using the MRC, an HRC block is used. This approach is mainly motivated by two reasons. First, the modularity of the HRC block allows the hysteresis curve to be made arbitrarily complex by adding more hysterons to the HRC block. Secondly, the HRC block resolves the causality issue raised by the MRC model, ensuring that the overall PZA system remains passive as previously mentioned. The modularity of the model is immediately seen when casting the PZA diagram as a Bond-Graph as shown in Figure 5b. In the diagrams the mechanical domain is represented in the blue dashed box, the electrical domain in the red dashed box, and the HRC block in the purple dashed box. In the Bond-Graph, grey dashed arrows allow for the additional connection of new hysterons to the HRC block. The Bond-Graph formulation is also convenient for identifying causality conflicts in the underlying mathematical dynamic relations [41]. A brief summary on Bond-Graph relations used in this work are presented in the Appendix A.

To derive the dynamic equations of the system the constitutive equations of the different components are used. Through the Bond-Graph it can be noticed that the C-store element in

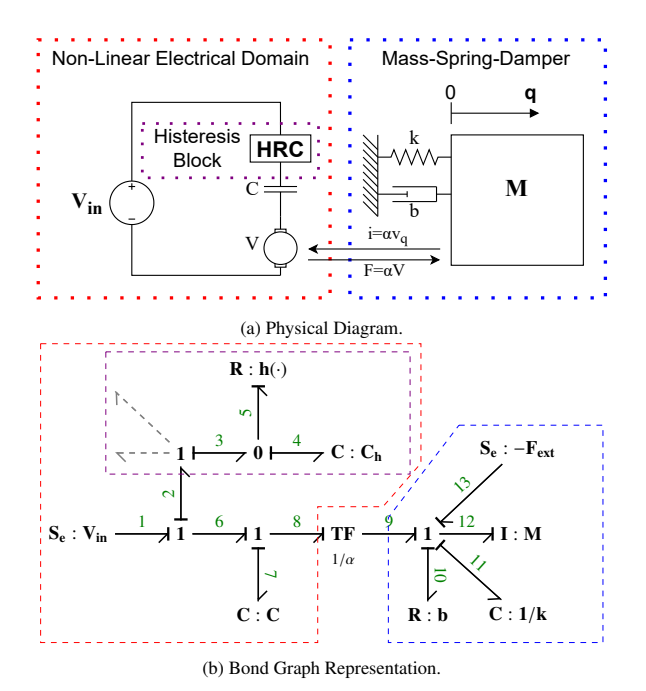


Figure 5: Piezoelectric actuator model diagram.

the electrical domain and the C-store element in the mechanical domain are interconnected with 1-junctions and a transformer, therefore they share a proportional flow. This implies that the dynamic equations for both components are proportional, $\dot{Q}_C = \alpha \dot{q}$, and consequently, the model can be immediately simplified by one state variable. The derived model has the following variables and parameters

- q the displacement for the PZA;
- k the elastic stiffness of the model spring;
- p the mechanical momentum of the PZA;
- *m* the mass of the PZA;
- b the damping of the model damper;
- α the model transducer ratio;
- Q_i the charge on the *i*th hysteron;
- C_i the capacitance of the ith hysteron;
- Q_C the charge on the external capacitor;
- C the capacitance of the external capacitor;
- h_i^{-1} the nonlinear damping on the *i*th hysteron;
- V_{in} the input voltage;
- F_{ext} the external force applied.

The dynamic equations are given by

$$\dot{Q}_{1} = -h_{1}^{-1} \left(\frac{Q_{1}}{C_{1}} \right) + \alpha \frac{p}{m}, \tag{3}$$

:

$$\dot{Q}_n = -h_n^{-1} \left(\frac{Q_n}{C_n} \right) + \alpha \frac{p}{m},\tag{4}$$

$$\dot{q} = \frac{p}{m},\tag{5}$$

$$\dot{p} = -\alpha \sum_{i=1}^{n} \frac{Q_i}{C_i} - kq - b\frac{p}{m} + \alpha V_{in} - F_{ext}.$$
 (6)

Notice that (3)-(4) correspond to the HRC block and have the structure of (1) driven by the current flow generated by the transductor. On the other hand (5)-(6) represent a mass-spring-damper system driven by the force generated by the transductor, external forces acting on the PZA and the force generated by the voltage applied to the PZA. It is important to notice that the dynamic equation of the capacitor outside of the HRC block, $\dot{Q}_C = \alpha \frac{P}{m}$, has not been included in the model, due to the state variable reduction previously mentioned. This is one of the important features of the Bond-Graph modeling formalism, because it helps to decide between different models or system configurations.

2.3. PH formulation of PZA and stability

An input affine PHS is defined as

$$\Sigma : \begin{cases} \dot{x} = [J(x) - D(x)] \frac{\partial H}{\partial x} + g(x)u \\ y = g(x)^T \frac{\partial H}{\partial x} \end{cases}$$
 (7)

where $x \in \mathbb{R}^n$ is the state and corresponds to the energy variables of the PZA, $H: \mathbb{R}^n \to \mathbb{R}$ is the Hamiltonian function and represents the stored electro-mechanical energy of the system, $J(x) \in \mathbb{R}^{n \times n}$ is a skew-symmetric interconnection matrix characterizing the coupling between energy storing elements, $D(x) \geq 0$, $D(x) = D(x)^T \in \mathbb{R}^{n \times n}$ is a positive semi-definite dissipation matrix that takes into account the electrical resistive elements and the mechanical damping elements, $u \in \mathbb{R}^m$ is the input vector which for the PZA corresponds to the voltage applied to its electrical terminals and $g(x) \in \mathbb{R}^{n \times m}$ is the input mapping. One of the features of PHS is that they are passive systems [42, 28]. This implies that they are asymptotically stable with respect to its unforced equilibrium. This follows immediately from the energy balance of (7)

$$\dot{H} = \frac{\partial H^T}{\partial x} \dot{x},$$

$$= -\frac{\partial H^T}{\partial x} D(x) \frac{\partial H}{\partial x} + y^T u.$$
(8)

This feature is important when considering nonlinear control design, in particular passivity based control (PBC) design methods which precisely exploit (8), such as control by damping injection or energy shaping [34]. In the case of PZA the unforced

equilibrium corresponds to a zero input voltage and zero external input force. However, due to the hysteresis of the system the equilibrium is not a single point but rather a set [40].

The PHS formulation can be directly obtained from a Bond-Graph [28]. In the case of the proposed PZA model it follows directly from the Bond-Graph of Figure 5.

Proposition 1. The PZA model (3)-(6) is a *passive* PHS (7) with state vector the energy variables $x = [Q_1, ..., Q_n, q, p]^T$, Hamiltonian function the electro-mechanical energy

$$H(x) = \frac{1}{2}x^T \mathcal{H}x,\tag{9}$$

where $\mathcal{H} = \text{diag}[1/C_1, \ldots, 1/C_n, k, 1/m]$, input vector the input voltage and the external mechanical force $u = \begin{bmatrix} V_{in} & F_{ext} \end{bmatrix}^T$, and structure matrices and input map

$$J = \begin{bmatrix} 0_{n \times n} & 0_{n \times 1} & \alpha_{n \times 1} \\ 0_{1 \times n} & 0 & 1 \\ -\alpha_{1 \times n} & -1 & 0 \end{bmatrix}, \qquad g = \begin{bmatrix} 0_{n \times 1} & 0_{n \times 1} \\ 0 & 0 \\ \alpha & -1 \end{bmatrix}$$
(10)

$$D(x) = \operatorname{diag} \begin{pmatrix} \left[\frac{C_1}{Q_1} h_1^{-1} \left(\frac{Q_1}{C_1} \right) \\ \vdots \\ \frac{C_n}{Q_n} h_n^{-1} \left(\frac{Q_n}{C_n} \right) \\ 0 \\ b \end{pmatrix} \right], \tag{11}$$

if the nonlinear damping function $h_i^{-1}(\cdot)$ maps $\mathbb{R}^+ \to \mathbb{R}_0^+$ and $\mathbb{R}^- \to \mathbb{R}_0^-$. Furthermore the forced equilibrium point

$$x^* = \begin{bmatrix} Q_1^* \\ \vdots \\ Q_n^* \\ \frac{\alpha}{k} \left(V_{in} - \sum_{i=1}^n \frac{Q_i^*}{C_i} \right) - \frac{1}{k} F_{ext} \\ 0 \end{bmatrix}, \tag{12}$$

where $h_i^{-1}(Q_i^*/C_i) = 0$, is globally asymptotically stable.

It is straightforward to verify that (3)-(6) correspond to the PHS defined in Proposition 1. Due the PHS structure the stability with respect to the unforced equilibrium is given by (8). However for inputs different from zero the stability must be proven.

Proof. The proof is composed of two parts: i) Passivity and ii) Global asymptotic stability to the equilibrium configuration.

i) To show the passivity of the proposed PH model, we can easily obtain that H(0) = 0 and the power balance equation can be computed

$$\dot{H}(x) = -\sum_{i=1}^{n} \frac{Q_i}{C_i} h_i^{-1} \left(\frac{Q_i}{C_i}\right) - b \left(\frac{p}{m}\right)^2 + y^T u.$$
 (13)

Since the nonlinear damping function $h_i^{-1}(\cdot)$ maps $\mathbb{R}^+ \to \mathbb{R}_0^+$ and $\mathbb{R}^- \to \mathbb{R}_0^-$, the $\sum_{i=1}^n \frac{Q_i}{C_i} h_i^{-1} \left(\frac{Q_i}{C_i}\right) > 0$ and and the damping coefficient b > 0 which imply

$$\dot{H}(x) = -\sum_{i=1}^{n} \frac{Q_i}{C_i} h_i^{-1} \left(\frac{Q_i}{C_i} \right) - b \left(\frac{p}{m} \right)^2 + y^T u < y^T u.$$
 (14)

Hence, the proposed PH model is passive.

ii). To prove the global asymptotic stability to the force equilibrium x^* , we consider the following Lyapunov function candidate

$$H_L(x) = \frac{1}{2}(x - x^*)^T \mathcal{H}(x - x^*), \tag{15}$$

which corresponds to the Hamiltonian (9) shifted with respect to the equilibrium (12). It is directly obtained that

$$H_L(x^*) = 0$$
, and $H_L(x) > 0$, (16)

for every x different to the equilibrium. Then by taking the time derivative of (15) it is obtained that

$$\dot{H}_{L}(x) = -\sum_{i=1}^{n} \frac{Q_{i} - Q_{i}^{*}}{C_{i}} h_{i}^{-1} \left(\frac{Q_{i}}{C_{i}}\right) - b \left(\frac{p}{m}\right)^{2}.$$
 (17)

The second term is always negative and corresponds to the mechanical dissipation by friction. The first term is the nonlinear dissipation induced by the HRC block. To prove that this term is negative let's split the domain of Q_i in three parts. The first subset S_1 includes every Q_i such that $h_i^{-1}(Q_i/C_i) = 0$. The second subset S_2 includes every positive Q_i that does not belong to S_1 . Finally, the third subset S_3 includes all the negative Q_i that does not belong to S_1 . By taking $Q_i \in S_1$ it is clear that

$$\frac{Q_i - Q_i^*}{C_i} h_i^{-1} \left(\frac{Q_i}{C_i} \right) = 0.$$

Then by taking $Q_i \in S_2$ we notice that $Q_i > Q_i^*$, which implies that $Q_i - Q_i^* > 0$. Therefore

$$\frac{Q_i - Q_i^*}{C_i} h_i^{-1} \left(\frac{Q_i}{C_i} \right) > 0,$$

Finally, by taking $Q_i \in S_3$ we notice that $Q_i < Q_i^*$, which implies that $Q_i - Q_i^* < 0$, thus

$$\frac{Q_i - Q_i^*}{C_i} h_i^{-1} \left(\frac{Q_i}{C_i} \right) > 0,$$

Then for every Q_i we have that

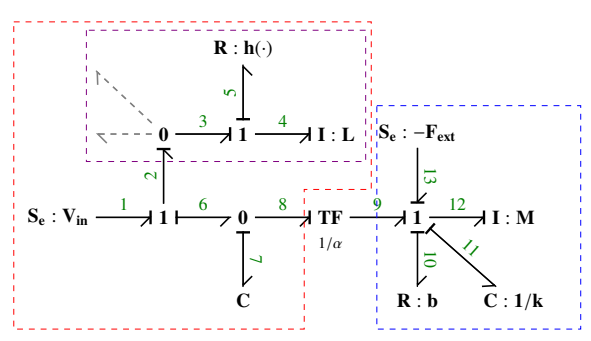
$$\frac{Q_i - Q_i^*}{C_i} h_i^{-1} \left(\frac{Q_i}{C_i} \right) \ge 0. \tag{18}$$

Consequently the first term of (17) is negative semi-definite and by Lyapunov's stability theorem the system is stable at (12). To prove the asymptotic stability of the system, the largest invariant set of $\dot{H}_L(x)=0$ is investigated. The set is obtained by taking the intersection between the zero set of h_1^{-1} and $\dot{x}=0$. The obtained set can be described as $S:\{x\in\mathbb{R}^{n+2}|h_i^{-1}(Q_i/C_i)=0$, $\delta=\delta^*$, $p=0\}$. Therefore using LaSalle invariance theorem it is concluded that the system is asymptotically stable with respect to the set of equilibrium points S.

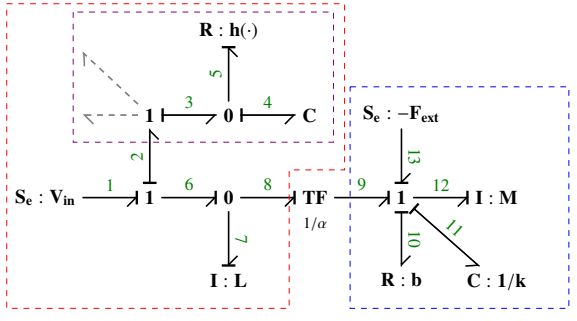
Since the proposed model is asymptotically stable with respect to a forced equilibrium it is convenient to model and study stability when considering a controlled actuation or when the PZA is used as a sensing element rather than an actuator.

2.4. Discussion

Different modeling considerations, which lead to alternative models, are briefly discussed in this subsection. The main discussion point is the hysteron choice and how it affects the electrical domain configuration.



(a) Series RL hysteron with capacitor (HRLC).



(b) Parallel RC hysteron with inductor (HRCL).

Figure 6: Alternative PZA models.

2.4.1. Hysteron choice

For the PA model of Proposition 1 a seemingly arbitrary choice has been made in the construction of the hysteron. The hysteron must be composed of a non-linear resistive component and an energy accumulating component. For the current PA model the hysteron is composed of a parallel connection of a capacitor and the non-linear resistance. This choice is not unique and alternative electrical configurations of the hysteron can be used. For instance, the energy accumulating component can be an inductor, or a series connection of the components could be considered. In the present paper the parallel RC hysteron is preferred since the resulting PA model is input affine and the causality of the underlying ODEs of the Bond-Graph of Figure 5 is such that all components are in series connection, including the mechanical domain components, which allows to reduce the order of the overall model. This choice does not affect the hysteresis modeling capacity as the same input/output were obtained with the four combinations of components in the hysterons. For the rest of the work the benefits of having an input affine model prevailed over the potential computational benefits that other hysterons models could have.

2.4.2. Electrical domain connection

It is important to notice that the series RL hysteron also renders an input affine model. Combining the different hysteron

options with different electrical configurations enables for the Bond-Graphs shown in Figure 6. The PZA model derived from the Bond-Graph of Figure 6a is one order higher than the one of Proposition 1. This is due to the series-parallel-series connection of the components, which does not allow to reduce the order of the dynamic system. The experimental validation of this model presents similar results to the proposed model, hence the additional state variable does not translate into a bigger benefit. On the other hand in the dynamic model derived from the Bond-Graph of Figure 6b the equilibrium point of the displacement does not depend on the input voltage, hence it is not able to model a step voltage input.

2.4.3. Applicability to other PZA

The proposed model was presented for a bidirectional PZA, but other applications can be discussed. By leveraging the modular formulation of the system, specific configurations of PZA can be studied using power preserving structures in the mechanical domain. For instance, in [4] a PZA is modeled as a second-order PHS and used to actuate a flexible optical fiber system. Even though the approach is simple it is underscored that there is a limitation in accurately capturing the hysteresis behavior of the PZA when changing the operation frequency. With the approach proposed in this paper this issue can be effectively addressed by interconnecting the PH hysteron based PZA model with the flexible optical fiber model while preserving the overall PH structure. This modular interconnection does not only enhance the modeling accuracy but also simplifies the control design. Additionally, in the case of asymmetric PZA, the non-linear damping function can be chosen with the property of obtaining an asymmetric hysteresis.

2.4.4. Temperature Dependence

The proposed model assumes isothermal operating conditions, i.e., constant temperature. However, in applications with large temperature gradients, the isothermal assumption is no longer valid. One of the advantages of the PH formulation is that, being a modular and multiphysical approach, it allows the incorporation of energy or entropy balances. This leads to Irreversible Port-Hamiltonian Systems (IPHS) [43, 44], a class of systems that define thermodynamically compatible PH formulations. For instance, in [25], a class of PZA is formulated as an IPHS by making the nonlinear resistance of the hysteron and the electromechanical coupling temperature-dependent, and by characterizing the entropy produced by the irreversible thermodynamic phenomena. Other hysteresis formulations, such as the Prandtl-Ishlinskii Hysteresis Model, have also been extended to account for thermodynamic effects through the use of nonlinear, temperature-dependent resistance functions [11].

3. Experimental Validation

The experimental validation of the proposed model is performed on a Thorlabs piezoelectric bender PB4VB2S [39] actuated by a high-voltage FLC Electronics A400DI linear amplifier. The displacement measurement is obtained by means of

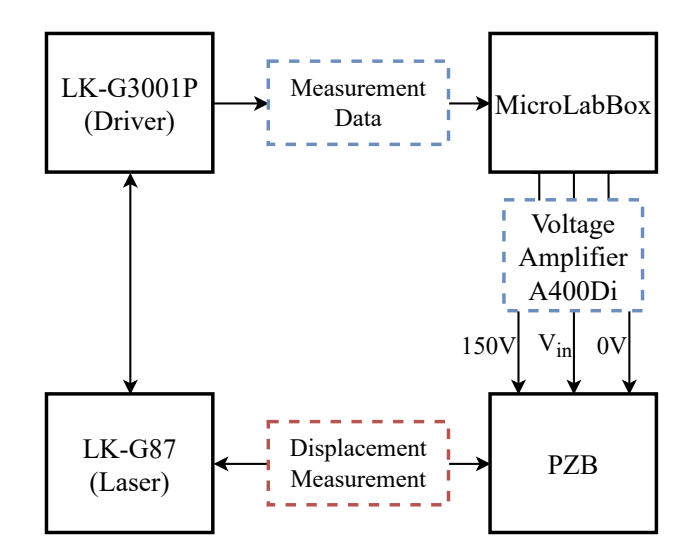


Figure 7: Experimental setup description.

a Keyence one-dimensional LK-G87 laser displacement sensor togehter with a Keyence LK-G3001P driver. The control unit is a dSpace MicroLabBox running with dSpace Control Desk. The control algorithm is programmed by Matlab. A diagram of the experimental setup is depicted in Figure 7, and the experimental arrangement is shown in Figure 8. The model identification uses four datasets. In each dataset, the external force applied to the piezoelectric bender is zero, and the input voltage is applied using a differential voltage. The identification datasets encompasses four 75V sinusoidal inputs at frequencies of 1Hz, 50Hz, 100Hz and 150Hz; and the validation datasets includes three 75V sinusoidal inputs at frequencies 10Hz, 25Hz and 75Hz.

3.1. Model identification

For the identification of the model, the mechanical parameters are first identified. The mass is obtained by weighting the PZA, m = 1.1104 g, and the PZA identified as a purely mechanical mass-spring-damper system the remaining mechanical parameters are k = 25.000 N/m and b = 3.7 Ns/m. In a second step, the transfer function of the complete model is obtained, considering (2) and linearizing it by setting the dead zone $d_i = 0$. The transfer function has relative order 2 with nzeros and n + 2 poles for n hysterons. For simplicity a model with two hysterons is considered. The transfer function is identified using quadratic cost minimization with the 'tfest' function of the 'System Identification Toolbox' in MATLAB. From the obtained transfer function the electrical parameters are estimated and taken as initial condition to perform a linear greybox estimation. This is done with the 'greyest' function from the 'System Identification Toolbox'. Following the linear identification, the non-linear parameters are obtained by solving a non-linear least square problem. This is implemented through the 'nlgreyest' function from the 'System Identification Toolbox' with the 'lsqnonlin' method from the 'Optimization Toolbox' in Matlab, a flowchart is presented in Figure 9 to summarize the model identification process. The obtained parameters

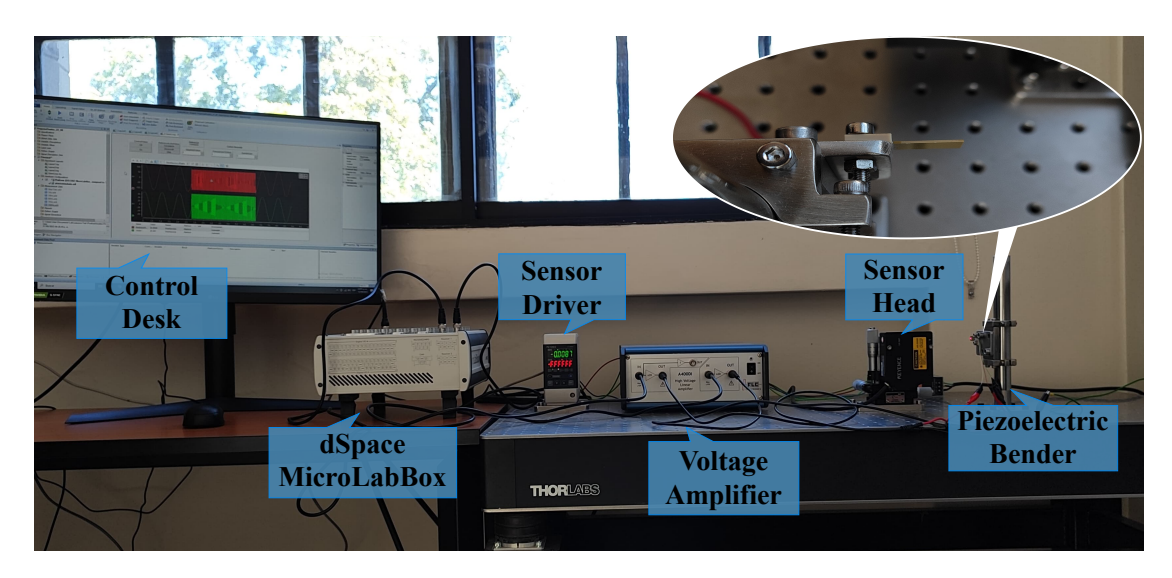


Figure 8: Experimental setup.

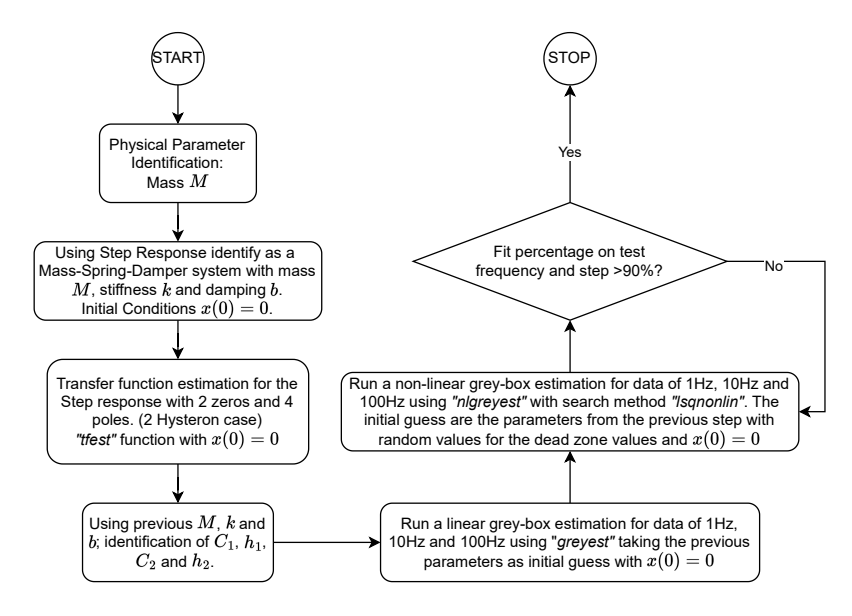


Figure 9: Identification flowchart.

are given in Table 1. Table 3 gives the fit percentages for different frequencies obtained by the 'compare' function in Matlab.

3.2. Comparison with a Bouc-Wen model

The results obtained with the proposed model are compared with the response of a Bouc-Wen (BW) model of the same order. The BW model is one of the most used mathematical models to model the dynamic behavior of the hysteresis in PZA [13, 14, 15, 16] and is characterized by the following set of non-linear ODEs [15]

$$\begin{split} \dot{h} &= A\dot{V}_{in} - \beta |\dot{V}_{in}|h - \gamma |h|\dot{V}_{in}, \\ \dot{\delta} &= \frac{P}{M}, \\ \dot{p} &= -k\delta - b\frac{P}{M} + K_{v}V_{in} - K_{h}h - F_{ext}. \end{split} \tag{19}$$

Table 1: Parameters for the PHS model.

Parameter	Value	Units
M	$1.0148 \cdot 10^{-3}$	[<i>kg</i>]
k	24579	[N/m]
b	3.7356	[Ns/m]
C_1	$5.6425 \cdot 10^{-7}$	[F]
C_2	$5.2125 \cdot 10^{-7}$	[F]
α	0.046311	[C/m]
ϱ_1^{-1}	0.6002	$[\Omega^{-1}]$
$ \varrho_2^{-1} $ $ d_1 $	$1.1528 \cdot 10^{-4}$	$[\Omega^{-1}]$
$d_1^{}$	14.7571	[V]
d_2	8.6838	[V]

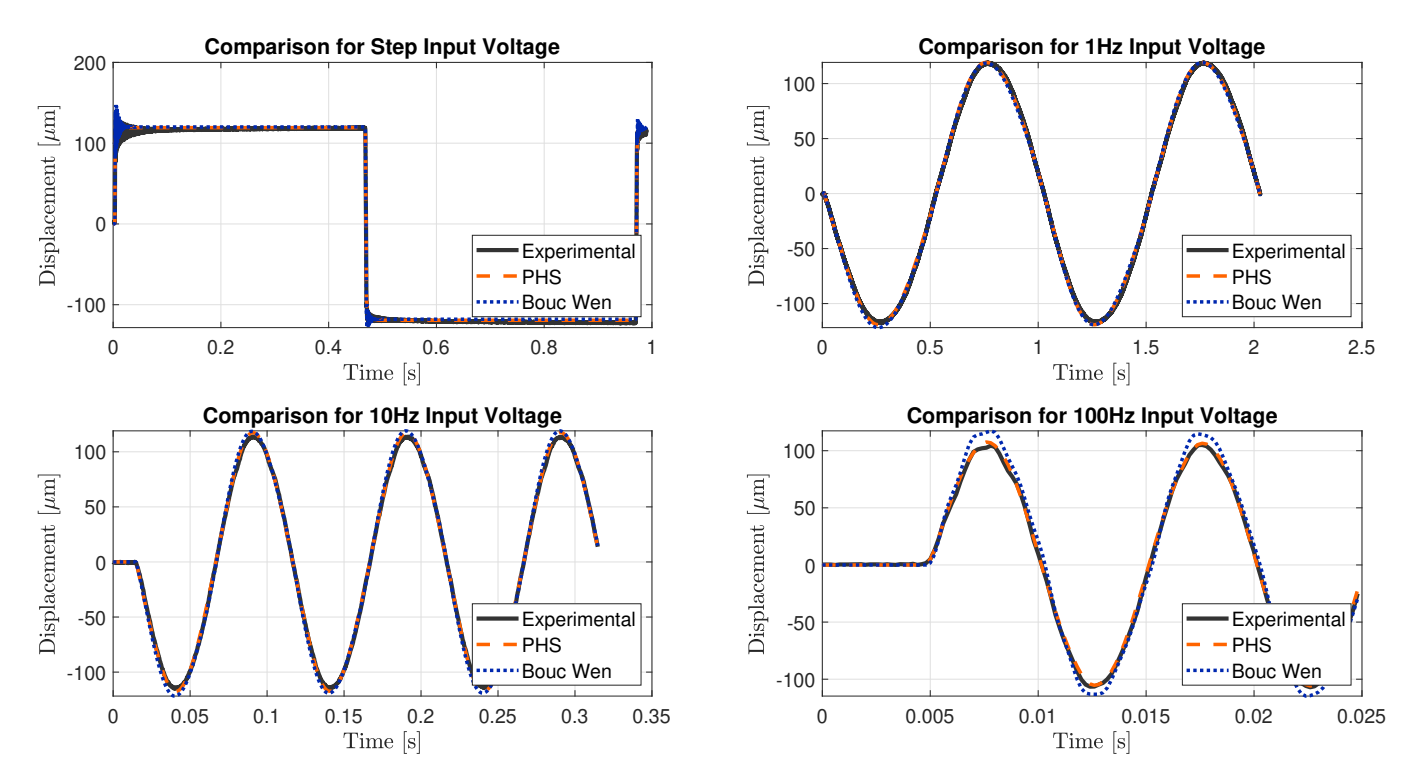


Figure 10: Response for identification inputs.

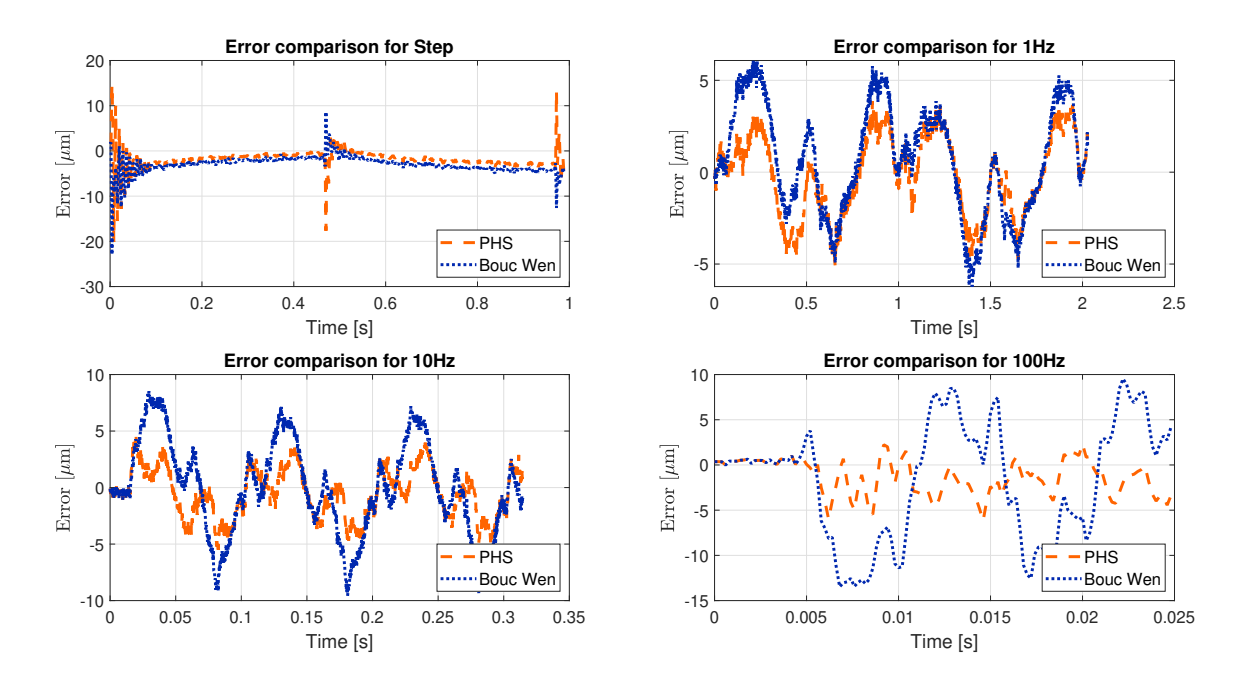


Figure 11: Error comparison for identification inputs.

Here the mass-spring-damper dynamics are completed with the dynamic of an internal state variable h which accounts for the hysteresis behavior of the actuator. The same procedure for parameter identification was employed as in the previous model, skipping the linear identification part. The obtained parameters are given in Table 2 and the fit percentage for sinusoidal inputs of different frequencies in Table 3. Figures 10, 11 and

12 show, respectively the time response for a step response and sinusoidal inputs of 1, 10 and 100Hz, the error between the simulated model and the experimental response, and the hysteresis curves of the corresponding inputs. While Figures 13 and 14 present the time response and error for a chirp input signal that goes from 1Hz to 100Hz.

A comparison between the proposed model and the BW

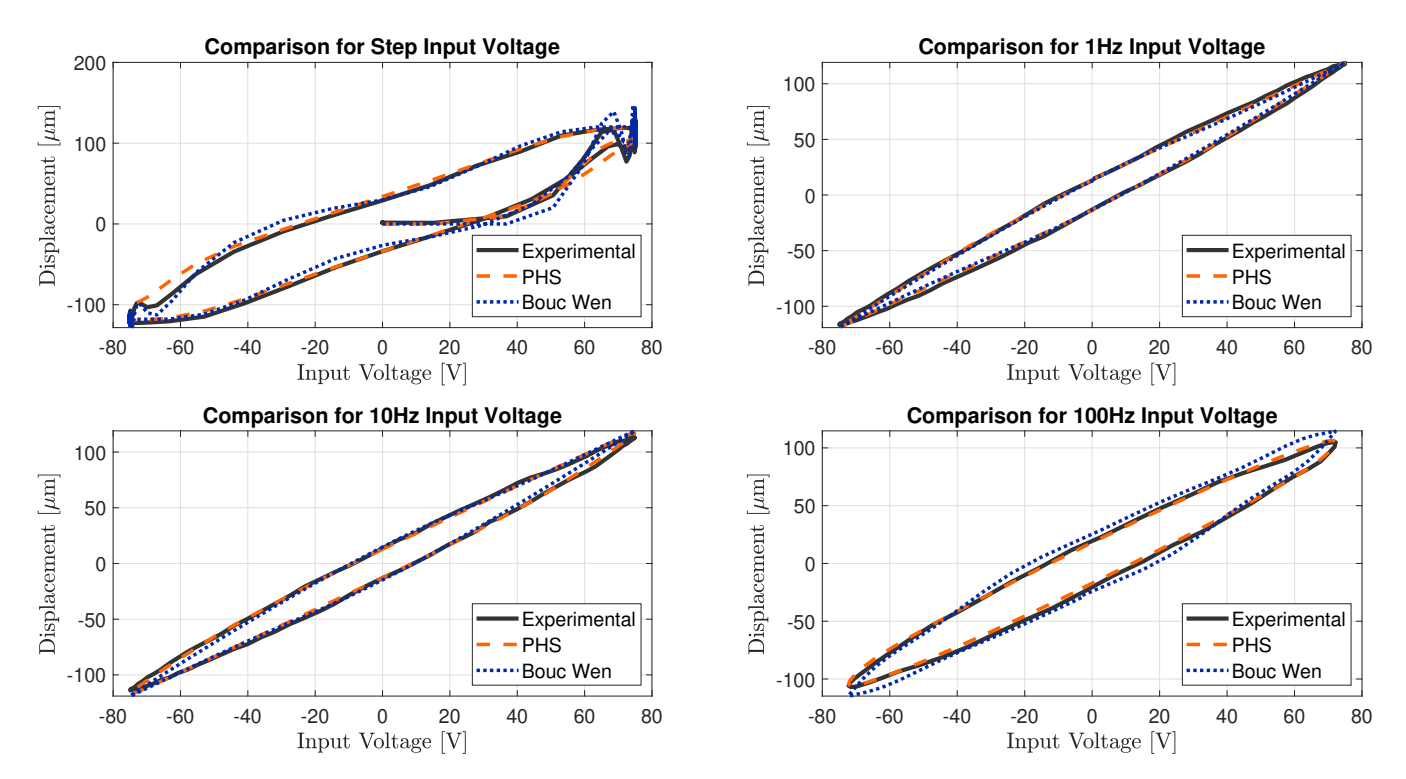


Figure 12: Hysteresis for identification inputs.

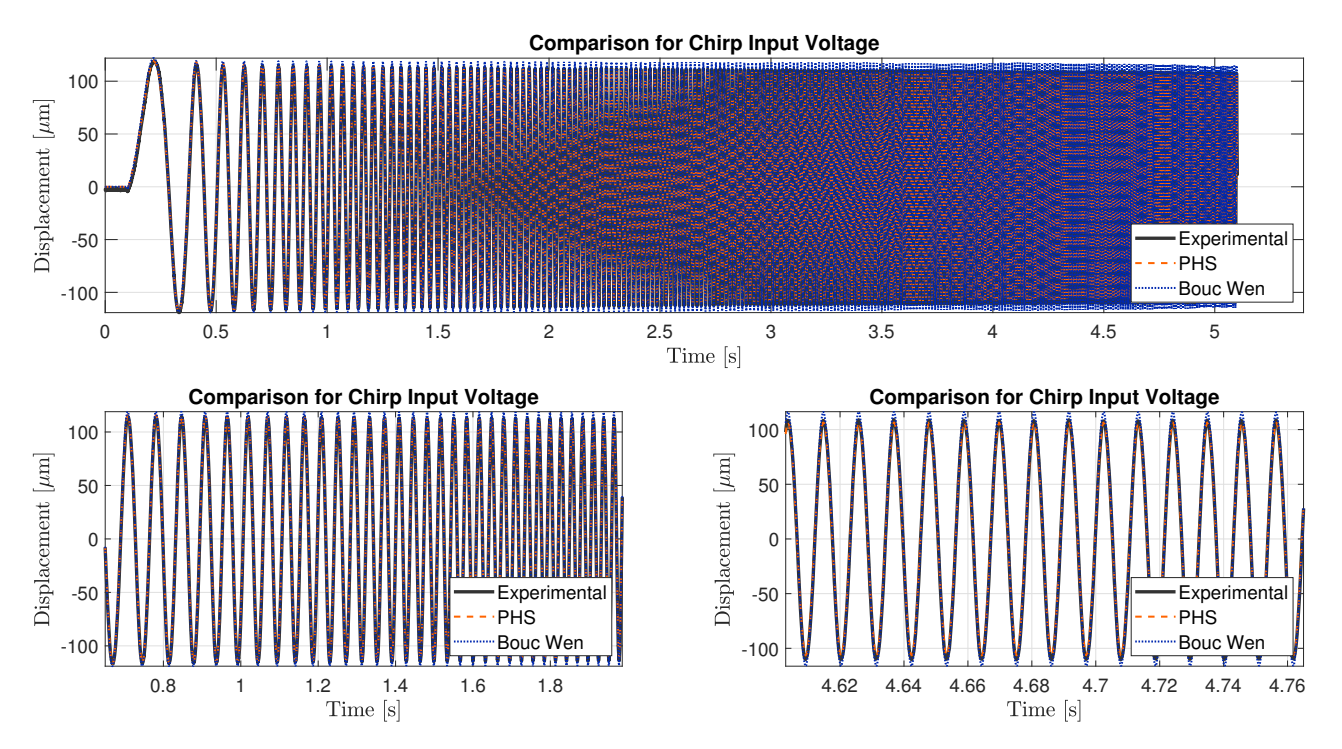


Figure 13: Chirp response of identified model.

model shows that both models have a high fit percentage, over 90%, for the sinusoidal inputs over the whole range of studied frequencies (1-150 Hz). However, while the BW model fit percentage decreases when the frequency increases, the PHS model fit percentage remains practically constant around 97%. In Figure 10 one can observe that at higher frequencies the BW

model struggles to accurately replicate the experimental data at the sinusoidal wave's extreme points. This is also highlighted in Figure 11, and quantified by the RMSE in Table 3 that presents the root mean square error (RMSE) for the identification and validation dataset. In Figure 12, it is observed that the hysteresis curves of both models closely resemble the hysteresis

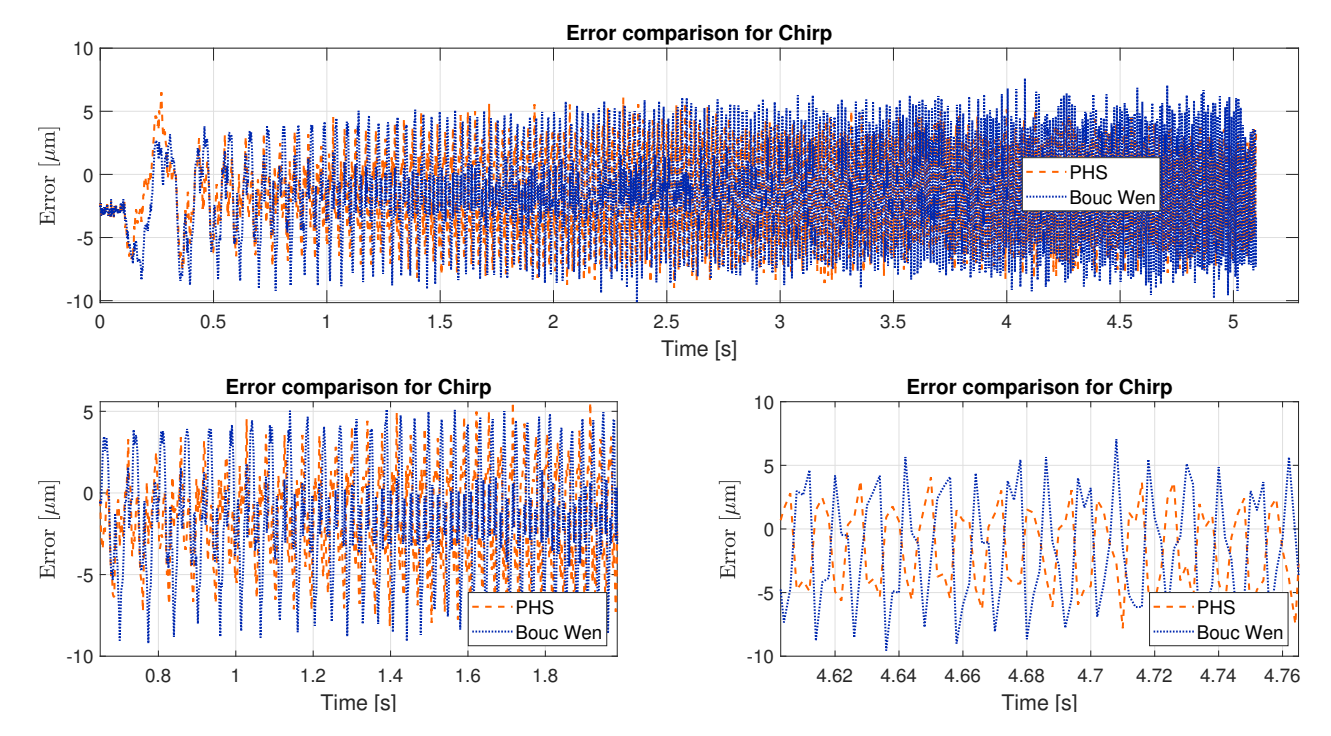


Figure 14: Error comparison for Chirp signal.

Table 2: Parameters for the Bouc-Wen model.

Parameter Value Units $9.4023 \cdot 10^{-4}$ M [kg]k 24579 [N/m]b 5.2 [Ns/m]0.008743 $[V^{-1}]$ \boldsymbol{A} $[V^{-1}]$ β 0.00637 $[V^{-1}]$ 0.0144905 γ K_{ν} 0.048676 [N/V] K_h 1.9767 [N]

curve of the PZA at lower frequencies. At higher frequencies however the proposed PHS model has a better fitness than the BW model. The improved high-frequency performance of the proposed PHS model arises from its power-preserving coupling between a mass-spring-damper system and an electrical domain that incorporates hysterons to represent hysteresis. This contrasts sharply with the Bouc-Wen model (and other common approaches), where the hysteresis component operates as a feedforward block-driven by input voltage but unaffected by the mechanical system. As a result, the dynamic coupling in the proposed model allows the mechanical domain to influence the hysteresis response, a feature absent in the BW model. On the other hand, for the step response the fit percentage and RMSE are very close and no real benefit is seen. Finally, in the case of a chirp signal in the range of the identified frequencies, the error grows in peak values for the BW as the frequency grows, meanwhile the proposed PHS model remains constant.

Finally, to illustrate that the model is rate-dependent, Figure

Table 3: Fit percentages summary for both models

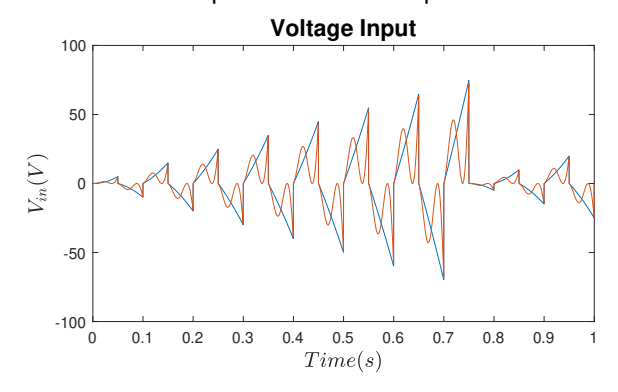
Experiment	Fit Percentage (%)		RN	RMSE (µm)	
2.1.1.0.1.1	PHS	Bouc-Wen	PHS	Bouc-Wen	
1 Hz	97.11	96.35	2.3251	2.9358	
10 Hz	97.23	94.97	2.2284	4.0418	
25 Hz	97.41	94.02	2.0335	4.6937	
50 Hz	96.59	93.06	2.6051	5.2988	
75 Hz	96.69	91.75	2.4579	6.1254	
100 Hz	96.99	90.80	2.2222	6.7942	
150 Hz	96.98	90.14	2.1947	7.1673	
Step	97.59	97.07	2.9342	3.5302	
Chirp	95.36	94.60	3.6480	4.2410	

15 shows an example using two input functions with the same extreme values but different rates of change. It can be seen that not only do the extreme displacements vary according to the input rate, but the intermediate values also differ.

4. Conclusion

A port-Hamiltonian system (PHS) model has been proposed to describe a large class of piezoelectric actuators with hysteresis. The proposed model comprises a mechanical mass-spring-damper subsystem and a nonlinear electrical subsystem which captures the hysteresis of the actuator. Furthermore, using Bond-Graphs, model configuration has been explored by investigating the causal interconnection between the energy storing components. The proposed model is a passive input-affine PHS asymptotically stable with respect to arbitrary equilibrium

Example PHS is rate-dependent



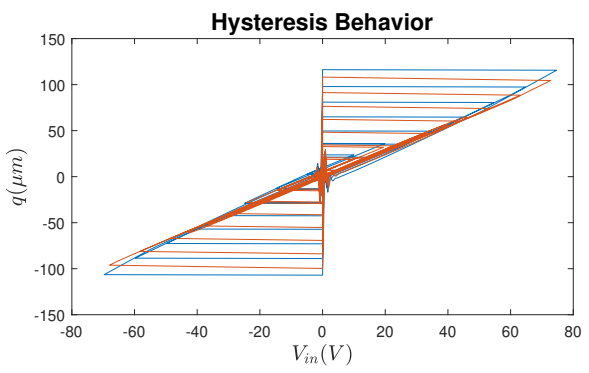


Figure 15: Rate-dependency example

configurations. The model showed high accuracy in experimental validations across a wide frequency range using a commercial piezoelectric actuator, achieving a fit percentage above 96.5% for sinusoidal inputs. The model was compared with a Bouc-Wen model of the same order, showing improved performances when working at high frequencies.

Future work shall investigate the use of the model for passivity based control techniques, the study of creep in the case of steady state regulation and the addition of the dynamic of the temperature in the model.

Appendix A. Bond-Graph Conventions

In the Bond-Graph (BG) formalism each bond is characterized by a couple of variables e(t) and f(t), related to power flows, and their corresponding energy variables $\dot{p}(t) = e(t)$ and $\dot{q}(t) = f(t)$, which characterize the dynamics of energy storing elements. The relation of power and energy variables in the mechanical and electrical domains are shown in Table A.4 and the elemental graphical relations and corresponding constitutive relations of BG are presented in Table A.5. See for instance [41] for a complete overview.

Acknowledgement

This work has been supported by the EIPHI Graduate School (contract ANR-17-EURE-0002) and Bourgogne-Franche-Comté Region and has been partially funded by the Chilean ANID

Table A.4: Power and energy variables.

Bond Grap	h	Mechanical De	omain	Electrical I	Oomain
Effort	e(t)	Force	F(t)	Voltage	V(t)
Flow	f(t)	Velocity	v(t)	Current	i(t)
Generalized Momentum	p(t)	Momentum	p(t)	Magnetic Flow	$\phi(t)$
Generalized Displacement	q(t)	Displacement	q(t)	Electric Charge	Q(t)

Table A.5: Basic BG relations.

Name	Graphical Representation	Constitutive Equation
0 Junction	→ 0 v-1	$\sum_{i=1}^{n} f_i = 0$ $e_i = e_j \ \forall i, j$
1 Junction	<u> </u>	$\sum_{i=1}^{n} e_i = 0$ $f_i = f_j \ \forall i, j$
Resistive element	$ \begin{array}{c} $	General: $e = \Phi_R(f)$ Linear: $e = Rf$
C store	$\longmapsto C:\Phi_C(\cdot)$	General: $q = \Phi_C(e)$ Linear: $q = Ce$
I store	$\longrightarrow I:\Phi_I(\cdot)$	General: $p = \Phi_I(f)$ Linear: $p = If$
Transformer	$ \begin{array}{ccc} & & & & & & & & & & \\ & & & & & & & & &$	$f_1g = f_2 \text{ and } e_1 = ge_2$
Effort source	$Se: e_s(t) \longrightarrow$	$e = e_s(t)$

sponsored projects FONDECYT 1231896, BASAL AFB240002 and ECOS220040.

References

- M. Senousy, R. K. N. D. Rajapakse, D. Mumford, M. S. Gadala, Self-heat generation in piezoelectric stack actuators used in fuel injectors, Smart Materials and Structures 18 (4) (2009).
- [2] F. Stefanski, B. Minorowicz, J. Persson, A. Plummer, C. Bowen, Non-linear control of a hydraulic piezo-valve using a generalised Prandtl–Ishlinskii hysteresis model, Mechanical Systems and Signal Processing 82 (2017) 412–431.
- [3] Y. Tian, K. Cai, D. Zhang, X. Liu, F. Wang, B. Shirinzadeh, Development of a XYZ scanner for home-made atomic force microscope based on FPAA control, Mechanical Systems and Signal Processing 131 (2019) 222–242.
- [4] E. P. Ayala, Y. Wu, K. Rabenorosoa, Y. Le Gorrec, Energy-based modeling and control of a piezotube actuated optical fiber, IEEE/ASME Transactions on Mechatronics (2022) 1–11.
- [5] A. Rajiv, Y. Zhou, J. Ridge, P. G. Reinhall, E. J. Seibel, Electromechanical model-based design and testing of fiber scanners for endoscopy, Journal of Medical Devices 12 (4) (09 2018).
- [6] W. Yang, S.-Y. Lee, B.-J. You1, A piezoelectric actuator with a motiondecoupling amplifier for optical disk drives, Smart Materials and Structures 19 (6) (2010).
- [7] H. Song, G. Vdovin, R. Fraanje, G. Schitter, M. Verhaegen, Extracting hysteresis from nonlinear measurement of wavefront-sensorless adaptive optics system. Optics Letters 34 (1) (2009) 61–63.
- [8] P. Liu, P. Yan, H. Özbay, Design and trajectory tracking control of a piezoelectric nano-manipulator with actuator saturations, Mechanical Systems and Signal Processing 111 (2018) 529–544.
- [9] Z. cheng Qiu, B. Wang, X. min Zhang, J. da Han, Direct adaptive fuzzy control of a translating piezoelectric flexible manipulator driven by a pneumatic rodless cylinder, Mechanical Systems and Signal Processing 36 (2013) 290–316.
- [10] J. Gan, X. Zhang, A review of nonlinear hysteresis modeling and control of piezoelectric actuators, AIP Advances 9 (4) (2019) 040702.
- [11] M. Savoie, J. Shan, Temperature-dependent asymmetric Prandtl-Ishlinskii hysteresis model for piezoelectric actuators, Smart Materials and Structures 31 (2022).
- [12] J. W. Macki, P. Nistri, P. Zecca, Mathematical models for hysteresis, SIAM Review 35 (1) (1993) 94–123. doi:10.1137/1035005.
- [13] M. Rakotondrabe, Bouc-Wen modeling and inverse multiplicative structure to compensate hysteresis nonlinearity in piezoelectric actuators, IEEE Transactions on Automation Science and Engineering 8 (2) (2011) 428-431.
- [14] D. Habineza, M. Rakotondrabe, Y. Le Gorrec, Bouc-Wen modeling and feedforward control of multivariable hysteresis in piezoelectric systems: Application to a 3-dof piezotube scanner, IEEE Transactions on Control Systems Technology 23 (5) (2015) 1797–1806.
- [15] T. Low, W. Guo, Modeling of a three-layer piezoelectric bimorph beam with hysteresis, Journal of Microelectromechanical Systems 4 (4) (1995) 230–237.
- [16] X. Fu, H. Gong, M. Lu, J. Zhou, J. Lin, Y. Du, R. Zhou, Piezoelectric hysteresis modeling of hybrid driven three-dimensional elliptical vibration aided cutting system based on an improved flower pollination algorithm, Micromachines 12 (12) (2021). doi:10.3390/mi12121532.
- [17] M. Goldfarb, N. Celanovic, A Lumped Parameter Electromechanical Model for Describing the Nonlinear Behavior of Piezoelectric Actuators, Journal of Dynamic Systems, Measurement, and Control 119 (3) (1997) 478–485.
- [18] M. Goldfarb, N. Celanovic, Modeling piezoelectric stack actuators for control of micromanipulation, IEEE Control Systems Magazine 17 (3) (1997) 69–79.
- [19] M. Rakotondrabe, Y. Haddab, P. Lutz, Quadrilateral modelling and robust control of a nonlinear piezoelectric cantilever, IEEE Transactions on Control Systems Technology 17 (3) (2009) 528–539.
- [20] P. Ge, M. Jouaneh, Tracking control of a piezoceramic actuator, IEEE Transactions on Control Systems Technology 4 (3) (1996) 209–216.

- [21] R. Georges Sabat, B. K. Mukherjee, W. Ren, G. Yang, Temperature dependence of the complete material coefficients matrix of soft and hard doped piezoelectric lead zirconate titanate ceramics, Journal of Applied Physics 101 (6) (2007) 064111.
- [22] R. Köhler, S. Rinderknecht, A phenomenological approach to temperature dependent piezo stack actuator modeling, Sensors and Actuators A: Physical 200 (2013) 123–132.
- [23] M. Al Janaideh, M. Al Saaideh, M. Rakotondrabe, On hysteresis modeling of a piezoelectric precise positioning system under variable temperature, Mechanical Systems and Signal Processing 145 (2020) 106880.
- [24] M. Momeni, N. Fallah, Meshfree finite volume method for active vibration control of temperature-dependent piezoelectric laminated composite plates, Engineering Analysis with Boundary Elements 130 (2021) 364– 378.
- [25] J. Caballeria, H. Ramirez, Y. Le Gorrec, An irreversible port-Hamiltonian model for a class of piezoelectric actuators, IFAC-PapersOnLine 54 (14) (2021) 436–441.
- [26] H. Zhang, Q. Yang, C. Zhang, Y. Li, Y. Chen, Temperature-dependent hysteresis model based on temporal convolutional network, AIP Advances (2024).
- [27] T. Wang, M. Noori, W. A. Altabey, Z. Wu, R. Ghiasi, S.-C. Kuok, A. Si-lik, N. S. Farhan, V. Sarhosis, E. N. Farsangi, From model-driven to data-driven: A review of hysteresis modeling in structural and mechanical systems, Mechanical Systems and Signal Processing 204 (2023) 110785.
- [28] V. Duindam, A. Macchelli, S. Stramigioli, H. Bruyninckx, Modeling and Control of Complex Physical Systems: The Port-Hamiltonian Approach, Springer Berlin, Heidelberg, 2009.
- [29] T. Voß, J. M. A. Scherpen, Port-Hamiltonian modeling of a nonlinear Timoshenko beam with piezo actuation, SIAM Journal on Control and Optimization 52 (1) (2014) 493–519.
- [30] A. Macchelli, A. van der Schaft, C. Melchiorri, Multi-variable port Hamiltonian model of piezoelectric material, in: 2004 IEEE/RSJ International Conference on Intelligent Robots and Systems (IROS) (IEEE Cat. No.04CH37566), Vol. 1, 2004, pp. 897–902 vol.1.
- [31] N. Calchand, A. Hubert, Y. Le Gorrec, Port Hamiltonian modeling of msma based actuator: toward a thermodynamically consistent formulation, IFAC Proceedings Volumes 45 (19) (2012) 260–264.
- [32] H. Ramirez, Y. L. Gorrec, N. Calchand, Irreversible port-Hamiltonian formulation of non-isothermal electromechanical systems with hysteresis, IFAC-PapersOnLine 51 (3) (2018) 19–24.
- [33] G. Rizzello, D. Naso, S. Seelecke, Hysteresis modeling in thermal shape memory alloy wire actuators: an irreversible port-Hamiltonian approach, in: 2019 IEEE 58th Conference on Decision and Control (CDC), 2019, pp. 7937–7943.
- [34] R. Ortega, A. van der Schaft, B. Maschke, G. Escobar, Interconnection and damping assignment passivity based control of port-controlled Hamiltonian systems, Automatica 38 (2002) 585–596.
- [35] B. Jayawardhana, R. Ouyang, V. Andrieu, Stability of systems with the Duhem hysteresis operator: The dissipativity approach, Automatica 48 (10) (2012) 2657–2662.
- [36] F. Ikhouane, V. Manosa, J. Rodellar, Bounded and dissipative solutions of the Bouc-Wen model for hysteretic structural systems, in: Proceedings of the 2004 American Control Conference, Vol. 4, 2004, pp. 3520–3525 vol.4. doi:10.23919/ACC.2004.1384457.
- [37] R. Tavares, M. Ruderman, Dissipation in suspension system augmented by piezoelectric stack: port-Hamiltonian approach, in: 2020 28th Mediterranean Conference on Control and Automation (MED), 2020, pp. 168–173.
- [38] D. Karnopp, Computer models of hysteresis in mechanical and magnetic components, Journal of the Franklin Institute 316 (5) (1983) 405–415.
- [39] Thorlabs, Piezoelectric Bimorph with Holder, 150 V, ±135 μm Travel, Thorlabs, Inc. (06 2020).
- [40] K. A. Morris, What is Hysteresis?, Applied Mechanics Reviews 64 (5) (2012) 050801.
- [41] D. Karnopp, D. Margolis, R. Rosenberg, System Dynamics: Modeling, Simulation, and Control of Mechatronic Systems, Wiley, 2012.
- [42] A. van der Schaft, Port-Hamiltonian systems: network modeling and control of nonlinear physical systems, in: H. Irschik, K. Schlacher (Eds.), Advanced Dynamics and Control of Structures and Machines, Springer, New York, 2004, pp. 127–168.
- [43] H. Ramirez, Y. Le Gorrec, Interconnection of irreversible port Hamilto-

nian systems, Automatica 170 (2024) 111846. [44] H. Ramirez, Y. Le Gorrec, An overview on irreversible port-Hamiltonian systems, Entropy 24 (10) (2022). doi:10.3390/e24101478.